Terminating states in the positive-parity structures of ^{67}As

R. Wadsworth,* N. S. Kelsall, and D. G. Jenkins
Department of Physics, University of York, Heslington, York, YO10 5DD, United Kingdom

I. Ragnarsson
Department of Mathematical Physics, Lund Institute of Technology, P.O. Box 118, S-22100 Lund, Sweden

S. M. Fischer
Department of Physics, DePaul University, Chicago, Illinois 60614, USA

D. P. Balamuth and P. A. Hausladen†
Department of Physics and Astronomy, University of Pennsylvania, Philadelphia, Pennsylvania 19104, USA

G. C. Ball
TRIUMF Laboratory, 4004 Westbrook Mall, Vancouver, British Columbia, Canada V6T 2A3

M. P. Carpenter, R. V. F. Janssens,‡ T. Lauritsen, C. J. Lister,§ and D. Seweryniak
Physics Division, Argonne National Laboratory, Argonne, Illinois 60439, USA

R. M. Clark, P. Fallon, A. O. Macchiavelli, and C. E. Svensson‖
Nuclear Science Division, Lawrence Berkeley National Laboratory, Berkeley, California 94720, USA

S. J. Freeman
School of Physics and Astronomy, University of Manchester, Manchester M13 9PL, United Kingdom

D. G. Sarantites
Department of Chemistry, Washington University, St. Louis, Missouri 63130, USA

(Received 4 May 2018; published 21 August 2018)

The energy levels and γ-ray decay scheme of the positive-parity states in the $T_z = \frac{1}{2}$ nucleus ^{67}As have been studied by using the ^{40}Ca(^{36}Ar,$2\alpha p$)^{67}As reaction at a beam energy of 145 MeV. Two new band structures have been identified which can be connected to the previously known levels. The results for these bands are compared with configuration-dependent cranked Nilsson–Strutinsky calculations. The good level of agreement between theory and experiment suggests that these structures can be interpreted in terms of configurations that involve three $g_{\frac{9}{2}}$ particles and that both possess noncollective terminating states.

DOI: 10.1103/PhysRevC.98.024313

I. INTRODUCTION

The concepts behind rotational band termination phenomena in nuclei are both well known and described in the literature; see, for example, Ref. [1]. Studies of high-angular-momentum states in proton-rich nuclei in the mass 60–75 region have revealed evidence for structures that reach their maximum spin state in different ways. For example, with only a few particles outside the ^{56}Ni core, the valence space configurations terminate in a noncollective state as seen, for example, in ^{62}Zn [2,3]. Furthermore, in ^{62}Zn, the same type of termination also occurs if one or two particles are excited across the $N = Z = 28$ shell gap. However, with more particles excited the configurations appear to reach their maximum spin state without significant loss of collectivity [3], which has been called nontermination [4]. This latter

*rw10@york.ac.uk
†Present address: Nuclear Security and Isotope Technology Division, Oak Ridge National Laboratory, Oak Ridge, Tennessee, 37830, USA.
‡Present address: Department of Physics and Astronomy, University of North Carolina at Chapel Hill, Chapel Hill, North Carolina 27599, USA and Triangle Universities Nuclear Laboratory, Duke University, Durham, North Carolina 27708, USA.
§Present address: Department of Physics and Applied Physics, University of Massachusetts Lowell, Lowell, Massachusetts 01854, USA.
‖Present address: Department of Physics, University of Guelph, Guelph, Ontario, N1G 2W1, Canada.

phenomenon has been experimentally confirmed in valence space configurations in the nucleus ^{74}Kr [4], with eighteen particles outside the ^{56}Ni core. Indeed, nontermination appears to be a general phenomenon for nuclei approaching the middle of the $Z, N = 28$–50 region; see, e.g., Ref. [5]. As discussed in Ref. [4], nontermination can be understood in terms of more particles (or particles + holes) outside closed shells leading to larger deformations and, thus, stronger couplings between the $\mathcal{N}$ shells. The present work is centered on the nucleus ^{67}As which lies at an intermediate point between the expected "terminating" nuclei with a few particles outside the ^{56}Ni core and nonterminating nuclei in midshell. ^{67}As is intermediate, both having $Z = 33$ midway between Zn ($Z = 30$) and Kr ($Z = 36$) and having eleven valence nucleons compared with six in ^{62}Zn and eighteen in ^{74}Kr. Thus, it presents an interesting and sensitive test case of models of high-spin nuclear band termination if such states can be populated.

The first states to be identified in ^{67}As resulted from the discovery of γ rays from the favored ($\alpha = \frac{1}{2}$) signature structure of the proton $g_{\frac{9}{2}}$ band [6]. This structure was subsequently extended up to a tentative spin of $(\frac{33}{2}^+)$ along with the measurement of the half-life of the $\frac{9}{2}^+$ state [7]. Further work on this nucleus [8] resulted in a minor change to the previously published energy-level and γ ray decay scheme associated with the $\pi g_{\frac{9}{2}}$ structure. Both of these works reported the existence of two $\frac{7}{2}^-$ states at energies of 697 and 1103 keV and an excited $\frac{3}{2}^-$ state at an energy of 68 keV. The only other information on negative-parity states in ^{67}As comes from a relativistic Coulomb excitation and inelastic-scattering experiment performed at the National Superconducting Cyclotron Laboratory (NSCL) at Michigan State University [9], which provided tentative assignments of $(\frac{9}{2}^-)$ and $(\frac{7}{2}^-)$ to states at 1242 and 720 keV, respectively. Given the large error quoted for the transition from the 720 keV level in this work it is possible that this may be the same state as the previously identified 697 keV level. In the present work, several new transitions have been added to the decay scheme, which have resulted in two high-spin positive-parity structures being observed up to tentative spins of $(\frac{45}{2}^+)$ and $(\frac{51}{2}^+)$. These results are discussed in terms of cranked Nilsson–Strutinsky (CNS) calculations [1,10,11].

II. EXPERIMENTAL DETAILS

A 145 MeV ^{36}Ar beam, provided by the ATLAS facility at Argonne National Laboratory, was used to bombard a 390-μg/cm^2-thick ^{40}Ca foil which had 113 and 97 μg/cm^2 flashes of gold in front and behind, respectively. The γ rays from the resulting fusion evaporation reactions were detected by the Gammasphere array [12]. The reaction chamber was located inside the array and contained the MICROBALL CsI charged-particle detector array [13], which was used to detect evaporated charged particles. The experimental setup also contained an array of 30 neutron detectors which replaced the most-forward Ge detectors in the Gammasphere array. However, the neutron detectors were not used during the present analysis, since ^{67}As was produced via the $(2\alpha, 1p)$ evaporation channel. During the experiment, the relevant data for the present work were collected by using a trigger condition that required more than four Compton-suppressed Ge detectors firing in prompt coincidence. The Ge detectors were calibrated for both energy and relative efficiency by using ^{152}Eu and ^{56}Co γ-ray calibration sources.

III. DATA ANALYSIS AND RESULTS

Emission of light charged particles from a compound nucleus in the mass-70 region results in a large broadening of the reaction product recoil cone, which, in turn, has a major effect on the resolution of the γ rays measured in the Ge detector array. To help overcome this problem in the current work, information from the CsI (MICROBALL) detector array such as particle identification and the hit pattern were used to provide both channel identification as well as a full kinematic reconstruction [14] for events involving the emission of two α particles and one proton, thereby enabling the Ge detector resolution to be significantly improved.

The Ge data were unpacked into triples events and sorted offline into an E_γ-E_γ-E_γ coincidence cube by using charged-particle gates of two α particles and one proton. The resulting cube was analyzed by using the RADWARE suite of programs [15]. By using double γ-ray gate coincidence events it was possible to deduce the level scheme presented in Fig. 1. Selected γ-ray spectra from this analysis are shown in Figs. 2

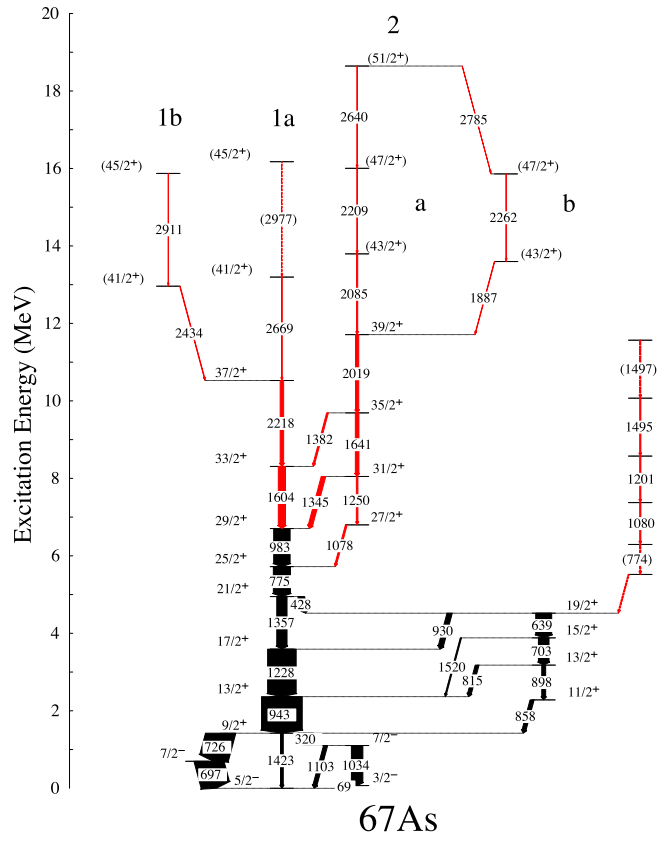

FIG. 1. Energy-level and γ-ray decay scheme for ^{67}As determined from the present work. The width of the transitions is proportional to the intensity of the γ rays. Transitions shown in red are new.

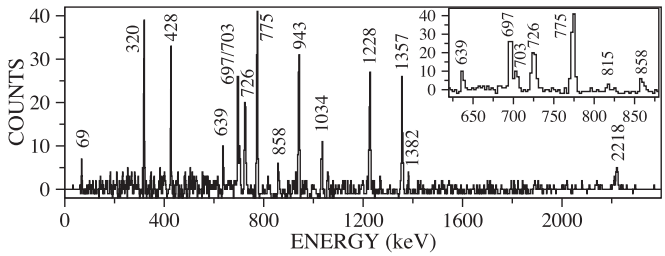

FIG. 2. γ-ray spectrum projected from the RADWARE cube discussed in the text. The figure shows the double-gated prompt-coincidence spectrum with gates on the 983 and 1604 keV transitions. The inset provides the same spectrum expanded in the region between approximately 620 and 880 keV for clarity.

and 3. These provide an indication of the cleanliness of the cube (which results from the use of high-multiplicity events along with analysis techniques described in Ref. [13]) and also inform on the level of statistics involved.

In addition to the above, the events were unpacked into double coincidence events and E_γ-E_γ matrices were produced with the same charged-particle conditions as those used to produce the cube discussed above. A directional correlation from oriented states (DCO) [16] matrix was constructed by

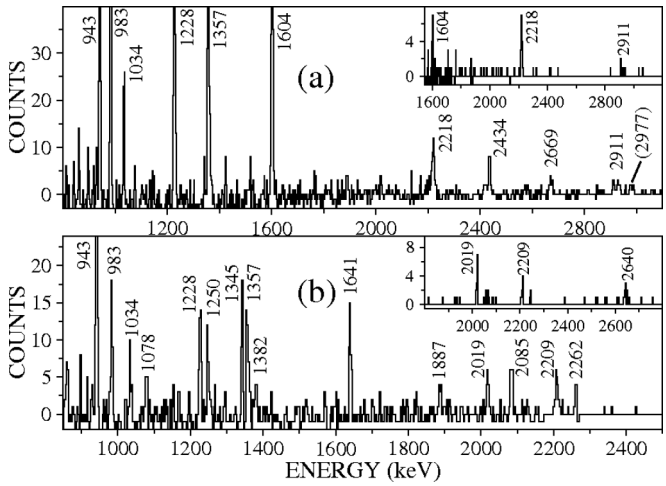

FIG. 3. Spectra showing the sum of prompt-coincidence double γ-ray gates taken from the RADWARE cube discussed in the text. (a) The spectrum is the sum of many double-gate combinations between all γ rays shown in Fig. 1, except the 69 keV transition, up to the 1604 keV line in band 1 and the 2218, 2434, and 2669 keV transitions. The upper part of this spectrum shows the transitions in bands 1a and 1b (see Fig. 1). The inset provides the upper portion of the spectrum from the sum of double gates between all γ rays in band 1 up to the 1604 keV transition, except the 69 keV line and the 2434 keV transition. This illustrates the upper part of band 1a. (b) Spectrum showing the sum of double-gate combinations between all transitions in the lower portion of band 1, except 69 keV, plus transitions in band 2 up to 2019 keV and the 2640 and 2785 keV transitions. The inset shows the upper portion of the spectrum containing the sum of double gates between the 775, 1078, 1345, 1250, 1641, and 2019 keV γ rays and the 2085 keV transition. This illustrates one of the two decay pathways seen in the upper part of band 2 in Fig. 1.

TABLE I. Energies, intensities, DCO ratios, and multipolarities of transitions observed in ^{67}As. DCO ratios were obtained by gating on the 943 keV $E2$ transition except where specified.

E_γ (keV)	I_γ	$R_{\rm DCO}$	Multipolarity
319.8(3)	35.4(26)	0.84(2)	$E1$
427.6(3)	15.4(11)	0.78(1)[a]	$M1/E2$
639.4(3)	39.1(26)	0.95(6)	$E2$
697.4(3)	71.4(25)	0.87(1)	$M1/E2$
703.4(3)	26.0(23)	[b]	$M1/E2$
726.0(3)	72.0(25)	0.79(1)	$E1$
774(1)			
774.5(3)	42.0(11)	1.09(2)	$E2$
815.4(3)	9.1(14)	0.93(5)	$M1/E2$
858.3(3)	9.7(17)	0.97(5)	$M1/E2$
898.2(3)	9.7(14)	0.89(6)[a]	$M1/E2$
930.2(5)	12.6(14)	0.93(4)	$M1/E2$
943.2(5)	100	1.07(2)[a]	$E2$
983.3(5)	40.3(20)	1.10(3)	$E2$
1034.1(5)	28.2(57)	1.03(4)	$E2$
1078.0(5)	4.1(4)	0.91(3)[a]	$M1/E2$
1080(1)			
1103.3(5)	10(3)	0.99(13)	$M1/E2$
1201(1)			
1228.4(5)	70.0(45)	1.12(2)	$E2$
1250(1)	3.8(4)	1.03(6)[a]	$E2$
1345.4(7)	10.9(9)	0.83(4)	$M1/E2$
1356.6(5)	26.3(8)	1.11(3)	$E2$
1382.4(5)	4(1)		$(M1/E2)$
1422.6(3)	6.7(3)	0.99(7)	$M2$
1495(1)			
1497(1)			
1520.2(7)	3.0(5)	1.0(1)	$M1/E2$
1603.6(5)	17.7(8)	1.08(5)	$E2$
1640.8(7)	8.8(7)	1.27(9)	$E2$
1886.6(7)	2.2(3)	1.1(2)[c]	$(E2)$
2018.8(7)	7.9(6)	1.12(6)[c]	$E2$
2085(1)	2.8(3)		
2209.4(7)	1.3(3)		
2218.0(7)	8.6(9)	1.13(9)[c]	$E2$
2261.7(7)	<1		
2434(1)	1.5(3)		
2640(1)	1.0(2)		
2669(1)	1.3(2)		
2785(1)	<1		
2911(2)	<1		
2977(2)	<1		

[a]Gate on 775 keV transition.
[b]Contaminated by 697 keV transition.
[c]Sum of gates on 943, 1228, 1357, and 983 keV transitions.

using Ge detectors from the $79^\circ - 101^\circ$ rings on the x axis and all other counters on the y axis to help deduce the multipolarity of the transitions. DCO ratios for known stretched-quadrupole–stretched-quadrupole transitions in ^{67}As were found to have a value of $\approx$1.1, while those for stretched-quadrupole–stretched-dipole transitions had a value of $\approx$0.8. The measured DCO ratios are presented in Table I, along with the γ-ray energies and intensities, which were extracted by using fitting routines in the xmlev RADWARE program.

IV. DISCUSSION

The decay scheme of Fig. 1 largely agrees with the most recently published level scheme presented in Ref. [8] up to spin $\frac{29}{2}^+$, the only differences being some small changes in the energies of two of the observed γ rays. All of these γ-ray-energy differences can be reconciled within the quoted experimental errors. In the present work, a 1604 keV transition is found to decay from the $\frac{33}{2}^+$ state in Fig. 1. The previously reported 1081 keV transition presented in Fig. 3 of Ref. [7] as decaying from this state is believed to correspond to either the 1078 keV transition in the present work, which as shown in Fig. 1 is in parallel with the 983 keV γ ray, or possibly the 1080 keV transition reported in the unconnected sideband (see Fig. 1). All γ rays in bands 1a and 1b above the $\frac{29}{2}^+$ level and in band 2 and the floating band on the right-hand side of Fig. 1 are new. Unfortunately, it was not possible to determine how, or exactly where, the floating band feeds into the $\frac{19}{2}^+$ state.

To help interpret the present experimental results we have used the configuration-dependent cranked Nilsson–Strutinsky (CNS) approach [1,10,11] with Nilsson (modified oscillator) potential parameters from Ref. [10]. Calculated energies of favored configurations are compared with the data from the present work in Fig. 4. The y axis of Figs. 4(a) and 4(b) present the experimental and theoretical energy, respectively, of a given state relative to a rotating liquid drop energy E_{rld}. The latter were calculated by using the prescription given in Ref. [11]; i.e., with the static liquid drop energy calculated with the Lublin–Strasbourg drop (LSD) model [17] and the rigid body moment of inertia with a radius parameter $r_0 = 1.16$ fm and a diffuseness 0.6 fm [18]. The notation used to label the calculated configurations in Fig. 4(a) is $[p_1p_2, n_1n_2]$ where $p_1(n_1)$ refers to the number of proton (neutron) $f_{\frac{7}{2}}$ holes and $p_2(n_2)$ is the number of proton (neutron) particles in the $g_{\frac{9}{2}}$ orbit.

For band 1, we require positive-parity configurations that yield a maximum spin of at least $\frac{49}{2}$. Such spins can be achieved with contributions from three $g_{\frac{9}{2}}$ particles. In the calculations, the [01, 02] configuration is the lowest such configuration at low-spin values, while the [02, 01] configuration occurs at similar energies for spins of ≈20 and above (see Fig. 4). The former configuration has $I_{\max} = \frac{49}{2}$ and has the following construction: $\pi(pf)^4_6(g_{\frac{9}{2}})^1_{4.5}\nu(pf)^4_6(g_{\frac{9}{2}})^2_8$, where the upper number refers to the number of particles in the specified orbits, the lower number is the maximum spin contribution from particles in those orbits, and (pf) effectively refers to the $p_{\frac{3}{2}}$, $f_{\frac{5}{2}}$ orbits, since the $p_{\frac{1}{2}}$ orbit is high in energy and, therefore, contributes little to the configuration. The full configuration for [02, 01] is $\pi(pf)^3_{4.5}(g_{\frac{9}{2}})^2_8\nu(pf)^5_{5.5}(g_{\frac{9}{2}})^1_{4.5}$ with signature $\alpha = \frac{1}{2}$ for the three pf orbit protons and $\alpha = -\frac{1}{2}$ for the five pf neutrons, yielding $I_{\max} = \frac{45}{2}$ for this specific configuration. As seen in Fig. 4, the close proximity of these two configurations above spin 20 suggests that the splitting observed at the top of band 1 in Fig. 1 (i.e., bands 1a and 1b) may result from a mixture of these two configurations.

Figure 4(c) presents the difference between the experimental and calculated energies, which come out as expected.

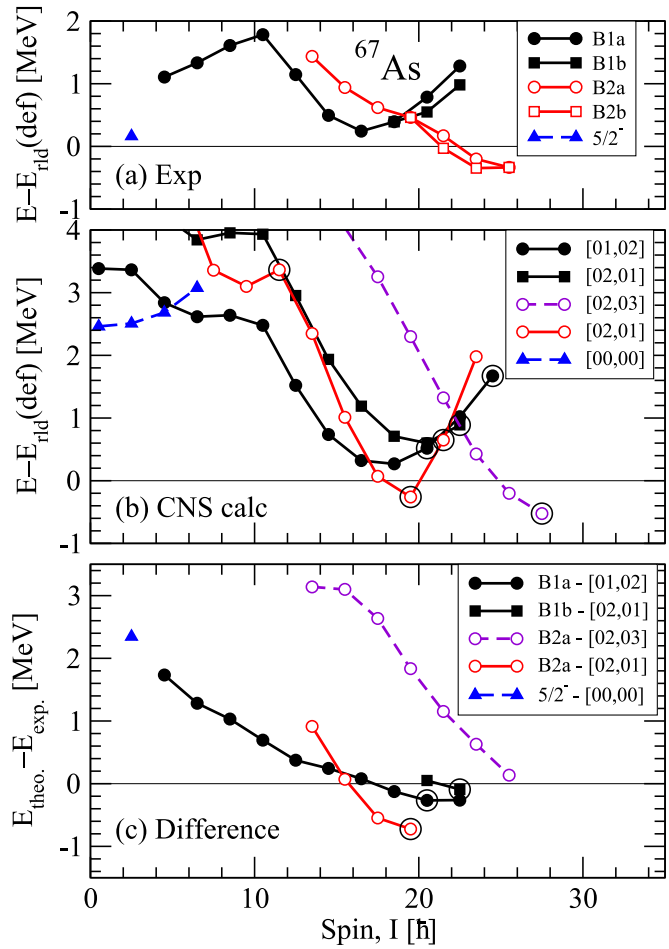

FIG. 4. (a) Experimental energies relative to a rotational liquid drop energy for bands 1a, 1b, 2a, 2b and the $\frac{5}{2}^-$ ground state. (b) Calculated energies for the configurations shown relative to the rotational liquid drop energy. Predicted noncollective terminating states ($\gamma = 60°$) are enclosed in large open circles. (c) Difference in energy between the calculated and experimental energies shown in panels (b) and (a).

Indeed, comparisons between paired and unpaired calculations in Refs. [19,20] suggest that the role of pairing at high spin is mainly a renormalization of the moment of inertia. The energy-difference curve for band 1 in Fig. 4(c) suggests that this is valid for all spin values in ^{67}As. Note also that the energy difference for the $\frac{5}{2}^-$ ground state follows the same smooth trend as band 1.

Coming back to the positive-parity states, the band crossing at $I \approx 10$ appears to be well described because the energy-difference curve [Fig. 4(c)] is smooth at all spin values, and especially around $I = 10$. In the calculations for $I \approx 10$, the deformation is calculated as $\varepsilon_2 \approx 0.30$, $\gamma \approx 30°$. The large value of γ means that the orbitals will be close to quantized around the rotation axis. Thus, for spin values up to $I = 8.5$, the two $g_{9/2}$ neutrons will be aligned in different directions (i.e., anti-aligned) giving only a small contribution (≈1ħ) to the total spin. However, at $I = 10.5$, they will both be aligned along the rotation axes contributing more than 6ħ, while the

fp protons and neutrons will have a negligible contribution. This provides a classic example of backbending as explained by Stephens and collaborators; namely, that two particles in a high-j shell align their spin vectors along the rotation axis; see, e.g., Refs. [21,22].

Band 2 is tentatively seen up to a spin of $(\frac{51}{2}^+)$, under the assumption that the top three transitions in branches 2a and 2b of Fig. 1 possess $E2$ multipolarity. Such high-spin, positive-parity states can only be formed in configurations involving five $g_{\frac{9}{2}}$ particles. In Fig. 4(a), comparison is made with the lowest such ([02, 03]) calculated configuration. It is clear from Fig. 4(c), however, that the difference between the experimental and calculated energies for this configuration is quite large and most likely too large for the level of agreement to be considered satisfactory. Indeed, a positive-parity band which is so low in energy strongly suggests that only three $g_{\frac{9}{2}}$ particles are involved in the configuration. In this respect, it is interesting to note that, above the $I^\pi = \frac{39}{2}^+$ state, band 2 branches, with each branch (labeled a and b in Fig. 1) having somewhat reduced intensity, suggesting that the structure of the band changes beyond this point. This assertion is further supported by Fig. 4(a), which shows evidence for a kink in the E-$E_{rld}(def)$ plot for both branches beyond spin $\frac{39}{2}$. Given that the statistics were insufficient to determine the DCO ratios of the uppermost transitions with any precision, it is possible that one or more of the transitions in each branch above the $\frac{39}{2}^+$ state in band 2 is actually dipole in character, thus the tentative spin assignments given to the levels in Fig. 1 in branches a and b of band 2 should be taken with some caution.

In this context, it is interesting to note that we can understand the $\frac{39}{2}^+$ level as associated with a favored noncollective terminating [02, 01] configuration with a detailed structure of $\pi(pf)^3_{4.5}(g_{\frac{9}{2}})^2_8\nu(pf)^5_{2.5}(g_{\frac{9}{2}})^1_{4.5}$. The maximum spin contribution shows that $\alpha = +\frac{1}{2}$ for both the $3pf$ protons and the $5pf$ neutrons; i.e., a total signature of $\alpha = -\frac{1}{2}$. This calculated [02, 01] band is compared with band 2 up to spin $\frac{39}{2}^+$ in Fig. 4. This assignment requires that the higher states above $\frac{39}{2}$ in band 2 are less favored; i.e., neither the 2085 nor the 1887 keV transition can have $\Delta(I) = 2$.

The reasons for the low-lying calculated aligned $\frac{39}{2}$ state can be seen from Fig. 5, which provides a tilted Fermi-surface plot for the configuration indicating the occupancy of the orbitals involved at the calculated deformation $\epsilon_2 = 0.28$ and $\gamma = 60°$, which corresponds to a noncollective oblate shape. The relatively high energy of the $f_{\frac{5}{2},\frac{3}{2}}$ states in Fig. 5 has been noted previously [23] and leads directly to a high energy for maximum spin configurations containing $3-5pf$ particles.

From Fig. 5, one can also understand why the highest spin state of the [01, 02] configuration in Fig. 4 is relatively high in energy. In this state, the high-lying $f_{5/2,3/2}$ state is occupied for both protons and neutrons. If both of these particles are moved to the $p_{3/2,-1/2}$ state, four units of angular momentum are lost, resulting in the $I = 20.5$ state which is more favored in energy and also noncollective, according to Fig. 4.

The above calculations were repeated by using the new parameters that were used to explain the configurations of terminating bands in the mass-60 region [3]. In the present case, the level of agreement between the experimental and theoretical levels in ^{67}As was found to be somewhat worse than that presented in Fig. 4. This suggests that the new parameters, which were used successfully to interpret structures in the

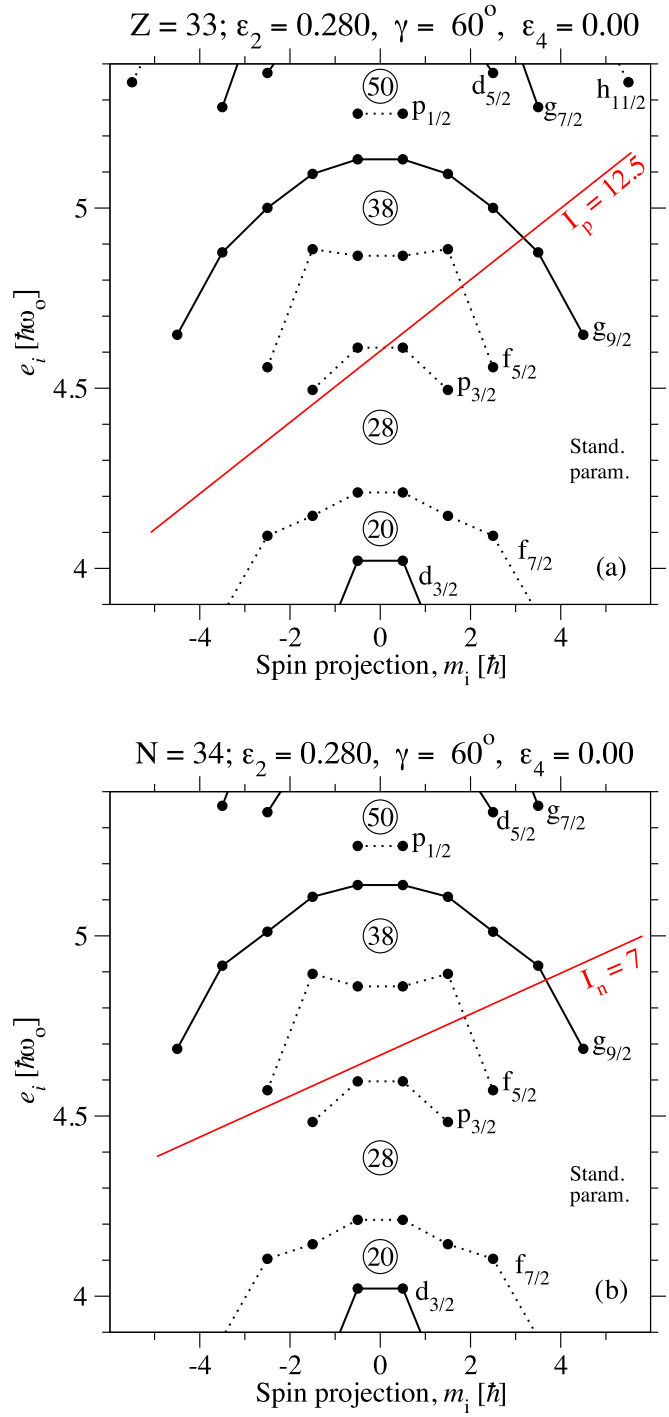

FIG. 5. Tilted Fermi-surface plots for protons (upper panel) and neutrons (lower panel) which illustrate how the favored $\frac{39}{2}^+$ state is built. Note that the $f_{\frac{5}{2},\frac{3}{2}}$ state is not occupied for either protons or neutrons. The states are labeled according to the dominant j shell in their wave functions, where solid lines are used for positive-parity states and dotted lines for negative-parity states.

mass-60 region, may only be valid for a limited range of nuclei in that region since, from the present work, the standard parameters seem better able to explain the observed positive-parity band structures in ^{67}As.

V. SUMMARY

The energy-level and γ-ray decay scheme of the positive-parity states in ^{67}As has been extended through the observation of two band structures that are connected to the previously known levels. These new data have been compared with configuration-dependent (constrained) cranked Nilsson–Strutinsky calculations. The good level of agreement between the data and calculations strongly suggests that the two new structures involve configurations containing three $g_{\frac{9}{2}}$ particles. The calculations also suggest that three of the levels involved are noncollective (i.e., $\gamma = 60^\circ$) terminating states. As would be expected, the first band crossing at $I \approx 10$ in the ground band is understood from the alignment of the spin vectors of two $g_{\frac{9}{2}}$ neutrons, but it is interesting to note that this seems to be well described in the present calculations, where pairing correlations are neglected. In future experiments it will be interesting to determine the multipolarity of the transitions above the $\frac{39}{2}^+$ state to confirm the interpretation of this structure.

ACKNOWLEDGMENTS

The authors would like to thank the staff at the ATLAS accelerator for providing the beam and John Greene for manufacturing the targets. This work was partially supported by the UK Science and Technology Facilities Council (STFC) (under Grants No. ST/L005727/1 and No. ST/P003885/1), the Natural Sciences and Engineering Research Council of Canada (NSERC), the US NSF, Department of Energy, under Contracts No. DE-AC02-06CH11357, No. DE-AC02-05CH11231, No. DE-FG02-95ER40934, and No. w-31-109-ENG38. S.M.F. also acknowledges support from the Research Corporation. This research used resources of ANL's ATLAS facility, a DOE Office of Science User Facility. TRIUMF is supported through a contribution from the National Research Council of Canada.

[1] A. Afanasjev, D. B. Fossan, G. J. Lane, and I. Ragnarsson, Phys. Rep. **322**, 1 (1999).
[2] C. E. Svensson, C. Baktash, G. C. Ball, J. A. Cameron, M. Devlin, J. Eberth, S. Flibotte, A. Galindo-Uribarri, D. S. Haslip, V. P. Janzen, D. R. LaFosse, I. Y. Lee, A. O. Macchiavelli, R. W. MacLeod, J. M. Nieminen, S. D. Paul, D. C. Radford, L. L. Riedinger, D. Rudolph, D. G. Sarantites, H. G. Thomas, J. C. Waddington, D. Ward, W. Weintraub, J. N. Wilson, A. V. Afanasjev, and I. Ragnarsson, Phys. Rev. Lett. **80**, 2558 (1998).
[3] J. Gellanki, B. G. Carlsson, I. Ragnarsson, and D. Rudolph, Phys. Rev. C **89**, 024301 (2014).
[4] J. J. Valiente-Dobon *et al.*, Phys. Rev. Lett. **95**, 232501 (2005).
[5] T. Steinhardt, J. Eberth, O. Thelen, H. Schnare, R. Schwengner, C. Plettner, L. Käubler, F. Dönau, A. Algora, G. deAngelis, A. Gadea, D. R. Napoli, M. Hausmann, A. Jungclaus, K. P. Lieb, G. A. Müller, D. G. Jenkins, R. Wadsworth, and A. N. Wilson, Phys. Rev. C **81**, 054307 (2010).
[6] T. F. Lang, D. M. Moltz, J. E. Reiff, J. C. Batchelder, Joseph Cerny, J. D. Robertson, and C. W. Beausang, Phys. Rev. C **42**, R1175 (1990).
[7] D. G. Jenkins, D. P. Balamuth, M. P. Carpenter, C. J. Lister, S. M. Fischer, R. M. Clark, A. O. Macchiavelli, P. Fallon, C. E. Svensson, N. S. Kelsall, and R. Wadsworth, Phys. Rev. C **64**, 064311 (2001).
[8] R. Orlandi, G. de Angelis, P. G. Bizzeti, S. Lunardi, A. Gadea, A. M. Bizzeti-Sona, A. Bracco, F. Brandolini, M. P. Carpenter, C. J. Chiara, F. DellaVedova, E. Farnea, J. P. Greene, S. M. Lenzi, S. Leoni, C. J. Lister, N. Marginean, D. Mengoni, D. R. Napoli, B. S. Singh, O. L. Pechenaya, F. Recchia, W. Reviol, E. Sahin, D. G. Sarantites, D. Seweryniak, D. Tonev, C. A. Ur, J. J. Valiente-Dobón, R. Wadsworth, K. T. Wiedemann, and S. Zhu, Phys. Rev. Lett. **103**, 052501 (2009).
[9] A. Corsi, J.-P. Delaroche, A. Obertelli, T. Baugher, D. Bazin, S. Boissinot, F. Flavigny, A. Gade, M. Girod, T. Glasmacher, G. F. Grinyer, W. Korten, J. Libert, J. Ljungvall, S. McDaniel, A. Ratkiewicz, A. Signoracci, R. Stroberg, B. Sulignano, and D. Weisshaar, Phys. Rev. C **88**, 044311 (2013).
[10] T. Bengtsson and I. Ragnarsson, Nucl. Phys. A **436**, 14 (1985).
[11] B. G. Carlsson and I. Ragnarsson, Phys. Rev. C **74**, 011302(R) (2006).
[12] I. Y. Lee, Nucl. Phys. A **520**, c641 (1990).
[13] D. G. Sarantites *et al.*, Nucl. Instrum. Methods Phys. Res., Sect. A **381**, 418 (1996).
[14] D. Seweryniak *et al.*, Nucl. Instrum. Methods Phys. Res., Sect. A **340**, 353 (1994).
[15] D. C. Radford, Nucl. Instrum. Methods Phys. Res., Sect. A **361**, 297 (1995).
[16] K. S. Krane, R. M. Steffen, and R. M. Wheeler, Atomic Data and Nuclear Data Tables **11**, 351 (1973).
[17] K. Pomorski and J. Dudek, Phys. Rev. C **67**, 044316 (2003).
[18] K. T. R. Davies and J. R. Nix, Phys. Rev. C **14**, 1977 (1976).
[19] Hai-Liang Ma, B. G. Carlsson, I. Ragnarsson, and H. Ryde, Phys. Rev. C **90**, 014316 (2014).
[20] C. M. Petrache, I. Ragnarsson, H.-L. Ma, R. Leguillon, T. Zerrouki, D. Bazzacco, and S. Lunardi, Phys. Rev. C **91**, 024302 (2015).
[21] F. S. Stephens, Rev. Mod. Phys. **47**, 43 (1975).
[22] S. G. Nilsson and I. Ragnarsson, *Shapes and Shells in Nuclear Structure* (Cambridge University Press, Cambridge, 1995), Chap. 11.
[23] J. Gellanki, D. Rudolph, I. Ragnarsson, L.-L. Andersson, C. Andreoiu, M. P. Carpenter, J. Ekman, C. Fahlander, E. K. Johansson, A. Kardan, W. Reviol, D. G. Sarantites, D. Seweryniak, C. E. Svensson, and J. C. Waddington, Phys. Rev. C **86**, 034304 (2012).